Earth, Planets and Space

FULL PAPER Open Access

Satellite orbit determination and time synchronization using GPS single-frequency observables in low and high solar activities

Tzu-Pang Tseng[1*], Wen-Hao Yeh[2], Yung-Fu Tsai[2], Tung-Yuan Hsiao[3], Yi-Hsuan Tsai[1], Pei-Jung Kuo[1], Kun-Lin Chen[2] and Yu-Shen Hsiao[4]

Abstract

We assess the orbit accuracy and time synchronization error using the L1 and C1 observables during the different solar activities. In general, GPS single-frequency (SF) observable can be used for commercial applications in satellite industry. The accuracy of satellite orbit determination using the SF observations is dominated by solar activities. The solar activities are indexed by the F10.7 value. The different solar activities lead to the ionosphere perturbation, triggering off the occurrence probability of ionospheric irregularities. The ionospheric irregularity affects the amplitude and phase of GPS signal. The affected amplitude and phase are indexed by the S4 value. We determine the GRACE satellite orbit using the SF GPS observations and compare the resulting orbit to that derived by dual-frequency observations for the effectiveness. The SF phase data are very sensitive to the variation in electron density and indirectly affects both the orbit accuracy and the time synchronization error. This is most likely caused by the phase ambiguity disturbed by the ionosphere. However, the C1 is relatively free from such a disturbance due to the strong signal-to-noise ratio (SNR) and the phase shift keying technique. The C1 performs the consistent solution over the low and high solar activities. However, this is not the case for the L1. The L1-derived orbit solution during the high solar activities is worse than that during the low solar activities. On the other hand, the time synchronization errors derived by the L1 and C1 are also different. The L1-derived time synchronization error has a relatively large perturbation as compared to the C1-derived one, which shows a consistent solution for a long-term period. This work suggests that the C1 observable is able to produce a consistent the orbit solution and time synchronization for the commercial applications of the satellite industry.

Keywords GNSS, LEO, Single frequency, POD, Time synchronization

*Correspondence:
Tzu-Pang Tseng
tzupangtseng@gs.ncku.edu.tw; tzupang.tseng@gmail.com
Full list of author information is available at the end of the article

Graphical Abstract

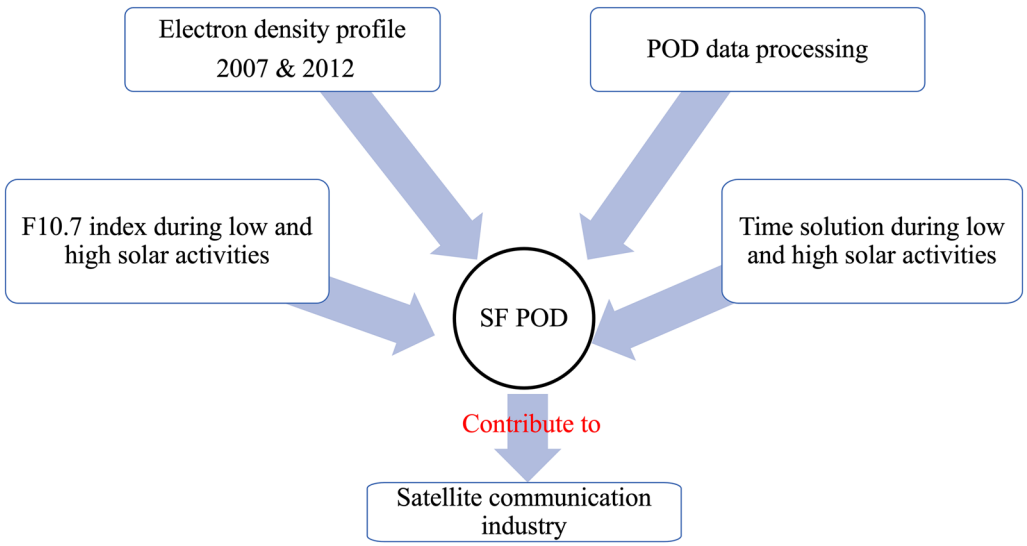

1 Introduction

Low earth orbit (LEO) Satellite industry has rapidly grown in the past decade. A variety of applications using the LEO satellites has been developed, ranging from the Earth observation, e.g., FORMOSAT-3/COSMIC and FORMOSAT-7/COSIMC-2 missions for atmospheric sciences and the GRACE mission for satellite geodesy, to the broadband connectivity service, e.g., OneWeb and Starlink. In addition, a LEO satellite network combining with a terrestrial 5G network is proposed for the future mobile communications (Kodheli et al. 2017; Guidotti et al. 2017; Ruan et al. 2018; Giambene et al. 2018; Kato et al. 2019). Such a non-terrestrial network requires both the orbit and the time synchronization information for the LEO satellite communication (SatCom) application.

For science-oriented satellites, the mission requirement of the positioning is more demanding and a dual-frequency receiver is equipped. However, this is not the case for the commercial satellites, which are mostly equipped with a GPS single-frequency (SF) receiver. In general, the GPS tracking data from the onboard receiver can be used for precise orbit determination (POD), which can be fulfilled using two approaches: kinematic approach and reduced-dynamic approach (Hwang et al. 2009; Tseng et al. 2017). The former is based on geometry approach, indicating that no force models are involved in the orbit determination. Conversely, the latter combines the GPS observations with the force models in the orbit determination procedure. Such a reduced-dynamic orbit solution produces a smoother orbit than a kinematic orbit solution does. In this sense, the reduced-dynamic orbit can compensate the orbit gaps happened to the kinematic orbit (Tseng et al. 2014). Such gaps are mostly associated with the number of satellites in view, e.g., less than 4. In comparison, the reduced-dynamic orbit is relatively continuous and is thus more favorable.

On the other hand, the time synchronization is part of the orbit determination and its error is dominated by the quality of the clock onboard the LEO satellite, namely clock stability (Tseng et al. 2014). Precise time synchronization is implemented by using the GPS clock correction in the orbit determination procedure in connection to the well-defined GPS time, which has an offset (namely leap seconds) with the Coordinated Universal Time (UTC). The offset information can be obtained from the GPS broadcast ephemeris. In a case of the SatCom application, the LEO satellite is regarded as a space relay terminal whose orbit and time synchronization are essential. The LEO orbit and time information can be integrated in a broadcast ephemeris format and then transmit to users for location and time estimations (Wang et al. 2021). This suggests that the LEO satellite as a space relay terminal requires the precise orbit and time synchronization information. For the time synchronization of the 5G communication, the end-to-end absolute time error is expected within ± 130 ns in support to a 260 ns time error of the signal propagation (Li et al. 2017; Mahmood et al. 2019).

However, the satellite orbit determination using the GPS SF observation is challenging due to the ionosphere activities. The GPS SF signal is very sensitive to the variation of

ionospheric electron density, which is associated with the solar activities. The variation of the ionospheric electron density is mainly retrieved by the radio occultation technique (Kursinski et al. 1997). The drastic gradient variation of the ionospheric electron density along the signal path causes the ionospheric scintillation, which is indexed by S4 value. Liu et al. (2016) demonstrated that the S4 index becomes more intensive over altitudes of 400–600 km during the high solar activities than that during the low solar activities.

In the SF data processing, the group and phase ionosphere correction (GRAPHIC) combination is used to mitigate the first-order ionosphere and is widely applied to satellite navigation and satellite orbit determination (Yunck 1996; Montenbruck and Ramos-Bosch 2008; Bock et al. 2009a). Although the first-order ionosphere is removed from such a combination, the unknown phase ambiguity is introduced, leading to the absolute time that is not able to be directly accessed. This is because the high correlation between the ambiguity parameters and clock parameters. For the SatCom or 5G communication application, accessing the absolute time is crucial for connecting the UTC (Li et al. 2017; Mahmood et al. 2019).

The objective of this work is to provide a consistent solution of satellite orbit and clock during the different solar activities. We use GRACE satellite as a case study to conduct the SF-derived orbit solution and time synchronization during different solar activities. The GRACE satellite is capable of receiving dual-frequency GNSS observables that can be used to derived a reference orbit for assessing the SF orbit solution. Besides, the GRACE satellite mission covers a long period from 2002 to 2016. Such a period is just between the 23rd solar cycle and the 24th solar cycle (Tseng et al. 2017). In Sect. 2, the fundamental theory of the POD using the GPS measurements is introduced. Electron density profiles in 2007 and 2012 is compared in Sect. 3. We also present a comparison between the SF-derived orbit solution of GRACE satellites in the 23rd solar cycle and the 24th solar cycle, as shown in Sect. 4. In addition, a comparison of the time synchronization errors during the different solar activities is targeted for the SatCom application in Sect. 5. The conclusion is given in Sect. 6.

2 POD data processing

In this section, we briefly introduce the concept of the POD using the GPS SF measurements. In practice, an initial orbit $\boldsymbol{r}_0$ is obtained the solution of the equation of satellite motion using the numerical integration. The equation of satellite motion is simply expressed with

$$\ddot{\boldsymbol{r}} = \ddot{\boldsymbol{r}}_0 + \ddot{\boldsymbol{r}}_{\boldsymbol{P}}, \tag{1}$$

where $\ddot{\boldsymbol{r}}$ denotes the total acceleration acting on the satellite; $\ddot{\boldsymbol{r}}_0$ denotes the acceleration caused by the attraction of the Earth's center of mass; $\ddot{\boldsymbol{r}}_{\boldsymbol{P}}$ denotes the acceleration caused by all potential perturbing forces, such as the inhomogeneous mass distribution of the Earth, N-body attraction, tidal effect, relativistic effects, and the non-gravitational forces, such as the solar radiation pressure and the air drag.

Table 1 summarizes both the GPS measurement models and the force models used in the SF POD of GRACE. The GRACE satellite orbit altitude is approximate to 450 km. In order to mitigate the ionosphere effect on the SF observation, we used the global ionosphere model (GIM) from CODE (Center for Orbit Determination in Europe) (Dach et al. 2015). Besides, the P1-C1 differential code bias (DCB) is applied to the SF POD. The EGM2008 is used as the a priori Earth's gravity field model for modelling the effect caused by the inhomogeneous mass distribution of the Earth (Pavlis et al. 2012). The JPL DE430 ephemeris is used for N-body effect. The standard models for both the tidal and the relativistic effects follow the recommendations of the IERS Conventions 2010. In addition, the relativistic correction is mainly based on the Schwarzschild correction. The non-gravitational forces are mainly associated with the satellite cross-sectional areas and satellite attitude control, which are difficult to be precisely modeled. Therefore, we use the stochastic pulses to model such non-gravitational forces or an instantaneous change of the accelerations. The satellite initial state vector, empirical parameters together with the stochastic pulses are estimated in the reduced-dynamic orbit determination procedure.

In general, the reduced-dynamic orbit determination mainly combines the force models with the GNSS measurements, where the GNSS measurement is used to constrain the orbit solution. The reduced-dynamic orbit is determined by a number of GNSS measurements that is dependent with the satellite initial state vector and force parameters (Beutler et al. 2006). The reduced-dynamic approach using the GNSS measurements can be expressed as follows:

$$\boldsymbol{l}(\boldsymbol{r}(t)) + \boldsymbol{v}(\boldsymbol{r}(t)) = \boldsymbol{l}(\boldsymbol{r}_0(t)) + \sum_{i=1}^{n} \frac{\partial \boldsymbol{l}(\boldsymbol{r}_0(t))}{\partial \boldsymbol{Z}_i} \cdot \left(\boldsymbol{Z}_i - \boldsymbol{Z}_{0,i}\right) \tag{2}$$

where $\boldsymbol{l}(\boldsymbol{r}(t))$ denotes the GNSS measurement $\boldsymbol{l}$ received in the orbit position $\boldsymbol{r}$ of the LEO satellite at time t, $\boldsymbol{v}$ denotes the measurement residual, $\boldsymbol{r}_0(t)$ denotes the initial orbit obtained from the solution of equation of the satellite motion, $\boldsymbol{Z}$ denotes the unknown parameter vector, $\boldsymbol{Z_0}$ denotes the initial values of the unknown parameters and the index i denotes the number of the

Table 1 Summary of GPS measurement and dynamic models used in SF POD of GRACE satellite

Items	
GPS measurement model	Single-frequency measurement: C1 code and L1 phase
	Ionospheric correction: CODE GIM model
	P1-C1 differential code bias
	GRACE PCOs + PCVs, igs08.atx[a]
	CODE GPS final orbit[b] and clock[c]
	0.1 Hz sampling rate
Attitude information	Attitude quaternions
Gravitational models	EGM2008 (120 × 120)[d]
	Solid Earth[e], Ocean tides[f] and pole tides (IERS2010, FES2004)
	Schwarzschild correction
	JPL DE430
Non-gravitational models	No air drag model
	No radiation pressure model
	Empirical parameters: 240 stochastic pulses in RTN[g]

[a] Rebischung et al. (2012)
[b] Dach et al. (2009)
[c] Bock et al. (2009b)
[d] Pavlis et al. (2012)
[e] Petit and Luzum (2010)
[f] Lyard et al. (2006)
[g] Radial, tangential, normal

unknown parameters; $\partial \boldsymbol{l}(\boldsymbol{r}_0(t))/\partial \boldsymbol{Z_i}$ is obtained from the solution of the variational equations.

As a final remark, the reduced-dynamic orbit can compensate those orbital gaps caused by the insufficient number of satellites in view, e.g., less than four satellites. In that case, the reduced-dynamic approach still can synchronize the time between the satellite and the ground user-end for the SatCom application. This is because the reduced-dynamic approach combines the force models with the GNSS ranging measurement which constrains the orbit solution to some extent, resulting in a stable orbit. In the following, we discuss the impact of the different solar activities on the SF POD.

3 Electron density profiles in 2007 and 2012

The electron density is highly correlated with the solar activities, which is generally indexed by *K*p index and F10.7 solar flux. The former is effective mostly for an orbit altitude below 200 km, e.g., GOCE satellite (Strugarek et al. 2019). However, for an orbit altitude of 450 km, e.g., GRACE, the F10.7 solar flux is the major factor affecting the ionosphere activities. Such an index is used to account for radio emission measurements from the Sun at a 10.7 cm wavelength. Figure 1 shows the 23rd solar cycle and the 24th solar cycle of F10.7 solar flux. The F10.7 Data download link is referred to https://spdf.gsfc.nasa.gov/pub/data/omni/low_res_omni/. In this work, we select two periods, DOY 273–279, 2007 and DOY 200–206, 2012, to assess the impact of the ionosphere associated with different solar activities on the SF POD of GRACE satellites. In Fig. 1, the F10.7 index over the first period of DOY 273–279, 2007 is on average about 70. In comparison, the second period of DOY 200–206, 2012 is approximate to 120, which is higher than the first period by 50. Such a difference in F10.7 may lead to different electron density profiles, indirectly affecting the SF POD solution.

The electron density profiles can be effectively derived from the radio occultation (RO). The RO products used in this work are collected from Taiwan Radio Occultation Process System (TROPS) (Yeh et al. 2022). The GPS signal is affected by the ionosphere, which causes a delay mainly resulted from the integration of the electron density along the signal path. Such an ionosphere delay is frequency-dependent and is related to the total electron content (TEC), which can be estimated using the geometry-free linear combination of the dual-frequency code measurements TEC_C and phase measurements TEC_p, respectively (Yeh et al. 2022):

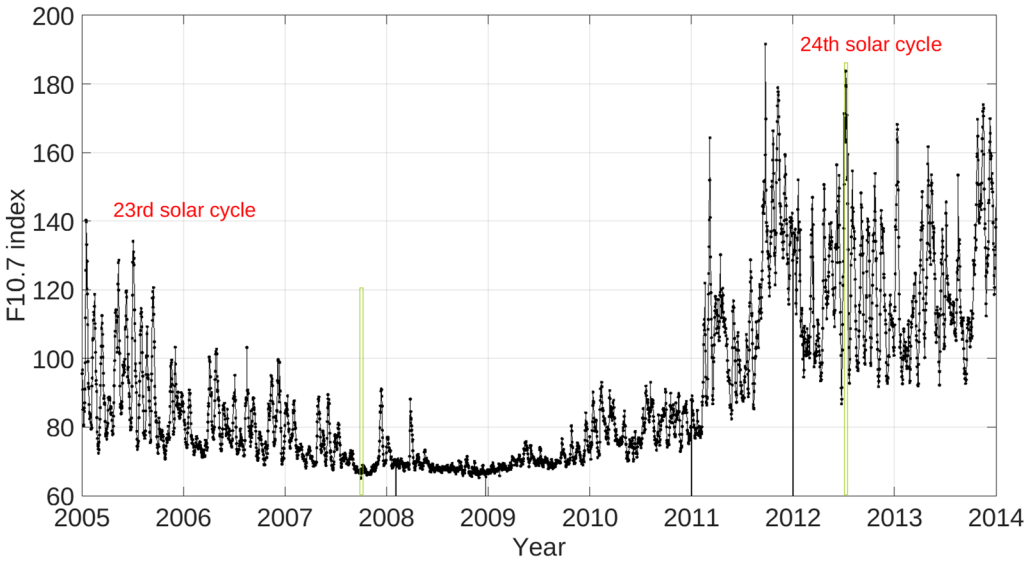

Fig. 1 Solar activities indexed by F10.7 over nine years, starting from 2005. This figure shows the F10.7 variations in 23rd and 24th solar cycles. Two periods of GRACE data are selected as shown in the green bar for a comparison of electron density profiles and its impact on the orbit determination

$$TEC_C = \frac{1}{40.31}\left(\frac{f_1^2 f_2^2}{f_1^2 - f_2^2}\right)\left[(P_2 - P_1) - \left(\Delta b_c^S + \Delta b_c^r\right)\right] + \varepsilon_c, \tag{3}$$

for a few minutes and can be used to derive the ionospheric electron density profile using the TEC, as follows (Schreiner et al. 1999):

$$TEC_L = \frac{1}{40.31}\left(\frac{f_1^2 f_2^2}{f_1^2 - f_2^2}\right)\left[(L1 - L2) - (\lambda_1 N_1 - \lambda_2 N_2) - (\Delta b_L^S + \Delta b_L^r)\right] + \varepsilon_L, \tag{4}$$

where P1 and P2 denotes the code measurement of the frequency L1 and L2, respectively; L1 and L2 denotes the phase measurement of the frequency L1 and L2, respectively; f_1 and f_2 denotes the frequency of L1 and L2, respectively; λ_1 and λ_2 denotes the wavelength of L1 and L2, respectively; N_1 and N_2 denotes the ambiguity of L1 and L2, respectively; Δb_c^S and Δb_c^r denotes the differential code bias (DCB) at the satellite end and at the receiver end, respectively; Δb_L^S and Δb_L^r denotes the phase bias at the satellite end and at the receiver end, respectively; ε_c and ε_L denotes the noise of code and phase measurements, respectively.

The electron density profiles are well retrieved using the FORMOSAT-3/COSMIC RO products (Yeh et al. 2022). We use Eqs. (1) and (2) to estimate the TEC between FORMOSAT-3/COSMIC satellites and GPS satellites over the two time spans: DOY 273–279, 2007 and DOY 200–206, 2012. The electron density profile derived by the RO technique is mainly based on the Abel transform (Phinney and Anderson 1968), which assumes that the ionosphere is spherically symmetrical. In general, an RO event lasts

$$\mathrm{N}(h_t) = -\frac{1}{\pi}\int_{h_t}^{h_{LEO}} \frac{dTEC/dp}{\sqrt{p^2 - h_t^2}}dp, \tag{5}$$

where N is the electron density; dTEC is the difference between a LEO-GPS link and its reference link; h_t is the altitude of the tangent point; h_{LEO} is the satellite orbit altitude; p is the altitude of the middle point between the LEO orbit altitude and the altitude of the tangent point. The ionospheric electron density profile is retrieved along the occultation path of the tangent point.

Figure 2 shows the mean electron density profiles in DOY 273–279, 2007 (blue) and DOY 200–206, 2012 (red). It is significant that the electron density in 2012 over an altitude ranging from 300 to 700 km is more intensive than that in 2007. This result agrees with that given by Liu et al. (2016). In addition, the different solar activities lead to the ionosphere perturbation, triggering off the occurrence probability of ionospheric irregularities (Chen et al. 2021). The ionospheric irregularity affects the amplitude and phase of the propagating GPS

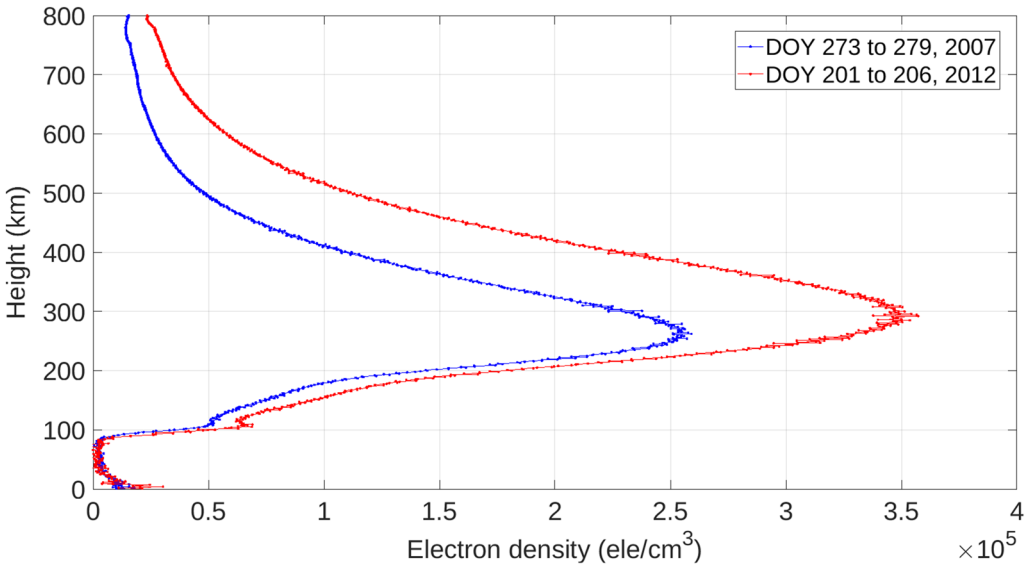

Fig. 2 The mean electron density profiles in DOY 273–279 2007 (blue) and DOY 200–206 2012 (red). These two periods are selected as shown in the green bar of Fig. 1

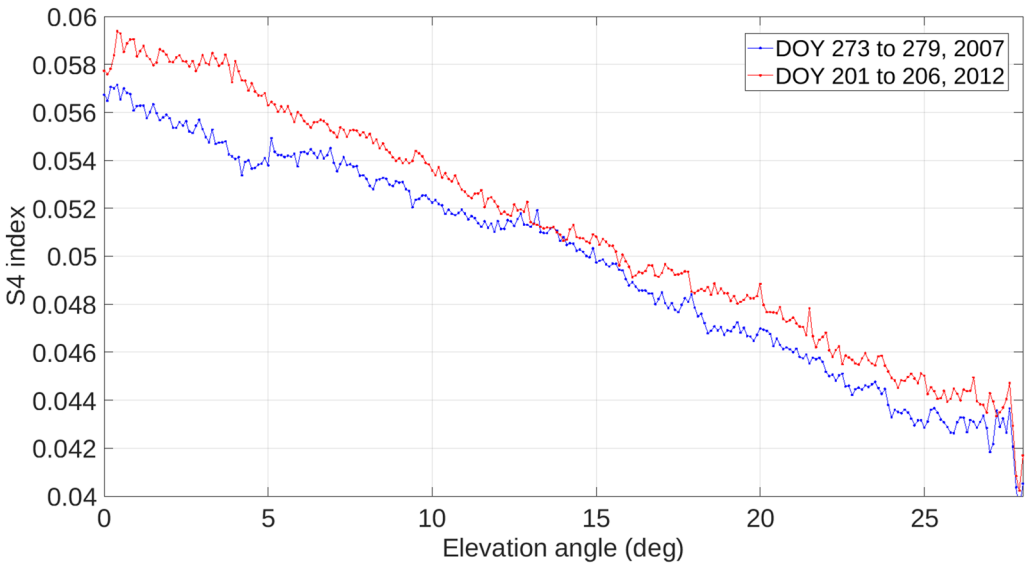

Fig. 3 S4 index of GPS L1 signal with the selected periods during the different solar activities: DOY 273–279 2007 (blue) and DOY 200–206 2012 (red)

signal, usually indexed by the S4 value (Briggs and Parkin 1963):

$$S_4 = \frac{\sqrt{\langle I^2 \rangle - \langle I \rangle^2}}{\sqrt{\langle I \rangle^2}}, \tag{6}$$

where I is the signal-to-noise ratio. The S4 index, which is computed at a 60 s span, is defined as a normalized ratio that accounts for the fluctuations of signal intensity to the mean one. Figure 3 shows the S4 index of L1 signal. Here the elevation angle is referred to the local vertical local horizontal (LVLH) frame (Tseng et al. 2012). The S4 index decreases with the elevation angle increased. This is due to the fact that the ionospheric gradient of the L1 signal with a low elevation is relatively large, as compared to that with a high elevation.

Note that both the electron density and the S4 index are derived by the FORMOSAT-3/COSMIC RO products.

With understanding of the ionospheric variations associated with the different solar activities, we determine the GRACE satellite orbit using the SF GPS observations (L1-only and C1-only) and compare the resulting orbit to that derived by dual-frequency observations for the effectiveness in the following. In addition, the time synchronization is part of the orbit determination procedure. Therefore, the time synchronization error is also assessed during the different solar activities.

4 SF POD during low solar activities and high solar activities

We use Bernese GNSS software to implement the reduced-dynamic orbit determination (Dach et al. 2015). In the SF POD, either the C1 or L1 measurement is used to firstly obtain the initial values of the satellite position and velocity, both of which are then adjusted by estimating the satellite state vector and force parameters. Note that the L1 phase ambiguity resolution is float. Different orbit solutions derived by the C1 and L1 are compared for assessments of orbit consistence during the different solar activities.

In order to assess the impact of the ionosphere activities associated with the electron density variation (Fig. 2) on the phase ambiguity, we also add the GRAPHIC observation in this data analysis. The GRAPHIC observation resulted from the combination of the L1 and the C1 and can be expressed as:

$$\mathrm{CL} = \rho_r^s + c\left(\Delta\bar{t}_r - \Delta t^s\right) + \delta I + \frac{1}{2}\left(\lambda_1 N_1 + \Delta b_{L1}^S\right) + m_{CL} + \varepsilon_{CL}, \tag{7}$$

with

$$\Delta\bar{t}_r = \Delta t_r + \frac{1}{2}\left(\Delta b_{c1}^r + \Delta b_{L1}^r\right), \tag{8}$$

$$A_{CL} = \frac{1}{2}\left(\lambda_1 N_1 + \Delta b_{L1}^S\right), \tag{9}$$

$$\delta I = \frac{1}{4}\Delta I_2 + \frac{1}{3}\Delta I_3, \tag{10}$$

$$m_{CL} = \frac{1}{2}(m_{c1} + m_{L1}), \tag{11}$$

$$\varepsilon_{CL} = \frac{1}{2}\left(\varepsilon_{c1} + \varepsilon_{L1} + \Delta b_{c1}^S\right), \tag{12}$$

where CL denotes the GRAPHIC observation; ρ_r^s denotes the geometry distance between the receiver and the satellite; c denotes the speed of light; Δt_r and Δt^s denotes the receiver clock offset and the satellite clock offset with respect to the GPS time, respectively; $\Delta\bar{t}_r$ is the receiver clock offset of the CL observation; ΔI_2 and ΔI_3 denotes the second- and third-order ionospheric delay, respectively; δI is the high-order ionospheric delay left for the CL measurement; Δb_{c1}^S and Δb_{c1}^r denotes the C1 hardware bias at the satellite and at the receiver, respectively; Δb_{L1}^S and Δb_{L1}^r denotes the L1 hardware bias at the satellite and at the receiver, respectively; A_{CL} is the CL phase ambiguity; m_{c1} and m_{L1} denotes the multipath of C1 and L1, respectively; m_{CL} is the CL multipath; ε_{c1} and ε_{L1} denotes the noise of C1 and L1, respectively; ε_{CL} is the CL noise.

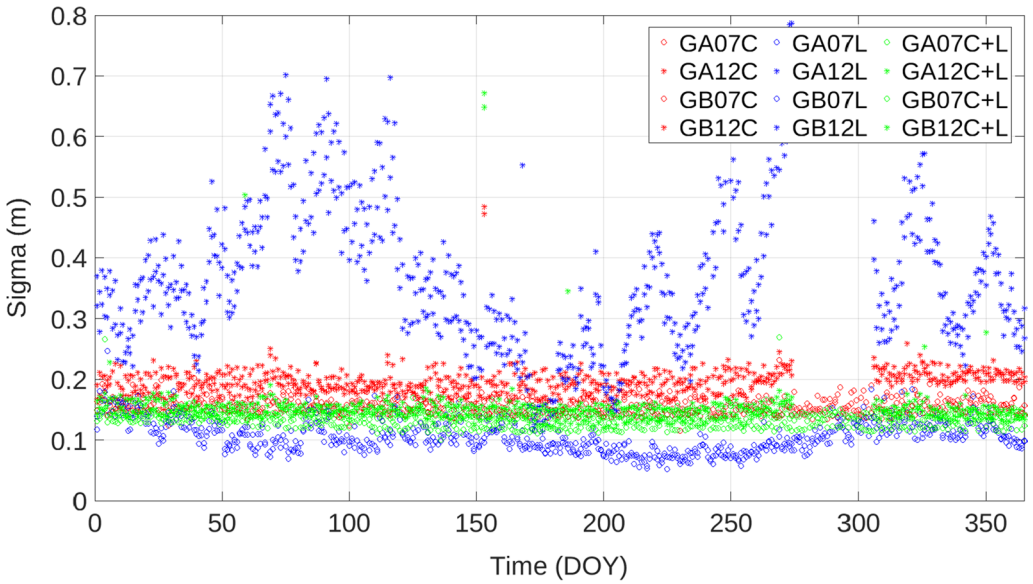

Fig. 4 A Posteriori sigma of the SF POD using L1 in blue, C1 in red and CL in green for 2007 (circle) and 2012 (asterisk). Here, C + L, C and L stands for the CL, C1 and L1, respectively; GA sand GB stands for the GRACE-A and GRACE-B, respectively

Figure 4 shows the a posteriori sigma of L1, C1 and CL for 2007 and 2012. The posteriori sigma stands for a quality indicator of the measurement after the least-squares estimation process. Here, the result from the CL is regarded as a reference solution for those from the L1 and C1. In Fig. 4, the C1 sigma in 2012 is better than the L1 one, showing a relatively consistent solution. This suggests that the C1 sigma is insensitive to the different solar activities and is close to the CL one. Besides, Hwang et al. (2010) demonstrated that the phase signal quality and multipath may be associated with the ionosphere activities. Table 2 summarizes the statistic information of the sigma for 2007 and 2012. Apparently, the L1 sigma is smaller than the C1 one by ~ 5 cm for 2007. However, this is not the case for the L1 sigma in 2012. The L1 sigma is larger and more divergent than the C1 one by ~ 20 cm in 2012. This is because the phase ambiguity resolution is affected by the ionospheric electron density (also see Fig. 6). In comparison, the C1 sigma is also affected by the high solar condition (year 2012) but is relatively insensitive, as compared to the L1 sigma.

In order to inspect the orbit performance, we used 2 weeks of GRACE-A GPS tracking data, DOY 273–279, 2007 and DOY 200–206, 2012, for the POD during different solar activities. The data from year 2007 and the data from 2012 are under the low and high solar activities, respectively, as shown in Fig. 1. Figure 5 shows the GRACE-A orbit difference derived by the CL, L1-only and C1-only with respect to the reference orbit during the low solar activities (LSA) and the high solar activities (HSA). Here, the GRACE reference orbit is derived by the GPS dual-frequency measurement. Kang et al. (2009) and Tseng et al. (2017) demonstrated that the GRACE orbit can be determined to cm level using the dual-frequency observations from GNSS satellites. Table 3 shows the statistic information of the orbit differences during the LSA and the HSA. In Fig. 5, the orbit difference derived by the CL is regarded as a reference for those derived by the L1 and C1. Overall, the L1-derived orbit difference is relatively perturbed as compared to the C1-derived one, in particular for the HSA period. In addition, the large orbit differences happen at the day boundary. This is because the orbit solution resulted from the daily batch job process, which leads to the phase ambiguity discontinuity at the day boundary. In Table 3, the orbit difference derived by L1 during the HSA is much worse than that during the LSA by ~ 1 m. The orbit accuracy in the L1 case from the LSA to the HSA ranges from 0.6 to 0.9 m in radial, 0.6–1.2 m in along-track and 0.4–0.5 m in cross-track. Note that the orbit difference derived by C1 during the HSA is consistent with that during the LSA. In the C1 case, the orbit accuracy is ~ 1, 0.7 and 0.4 m in the radial, along-track and cross-track, respectively. This may be due to the fact that the phase data are relatively sensitive to the ionosphere activity, which is mainly dominated by the variation of the F10.7 values. A strong ionosphere activity causes phase cycle slips, affecting the phase ambiguity parameter setup in the POD procedure, decreasing the degree of freedom and degrading the orbit accuracy. Note that the CL-derived orbit difference in the cross-track direction is more perturbed than both the C1- and L1-derived. This implies that an unknown perturbing force is introduced in the cross-track component when the CL is used. This is left for future works.

From Eq. (7) to Eq. (12), the CL observation is actually a phase measurement, which is free from the first-order ionospheric effect and mitigates the high-order effect. Besides, the CL has an ambiguity term A_{CL}, which is potentially affected by cycle slips and prevent the receiver clock connecting to the absolute time (see the following section). Note that the P1-C1 DCB is introduced in the SF POD, the term Δb_{c1}^{S} is cancelled out and the noise level of the CL is approximate to half of the C1. According to Bock et al. (2009a), the quality of the CL observation is mainly dominated by the code noise, implying that the orbit solution may be degraded if the code noise is larger than the ionosphere effect. That is, for a LEO satellite with an orbit height of ~ 450 km where the electron density is small (see Fig. 2), the quality of the SF POD using the CL might be dominated by the code noise rather than the ionosphere effect.

Figure 6 shows a ratio between the number of ambiguity and the number of observations for GRACE satellites. In the procedure of the satellite orbit determination, one phase ambiguity parameter is setup when a GPS signal is locked by the satellite until a cycle slip occurs or a new arc is started. A high ratio value means the relatively high occurrence of the cycle slip. In Fig. 6, the ratio is relatively

Table 2 Statistic information of the posteriori sigma of the SF POD using L1, C1 and CL for 2007 and 2012

	GRACE-A						GRACE-B					
Year	2007			2012			2007			2012		
Obs. type	C1	L1	CL	C1	L1	CL	C1	L1	CL	C1	L1	CL
RMS (cm)	14.9	10.7	14.3	19.3	38.9	15.5	14.2	9.6	12.5	17.8	33.1	14.2

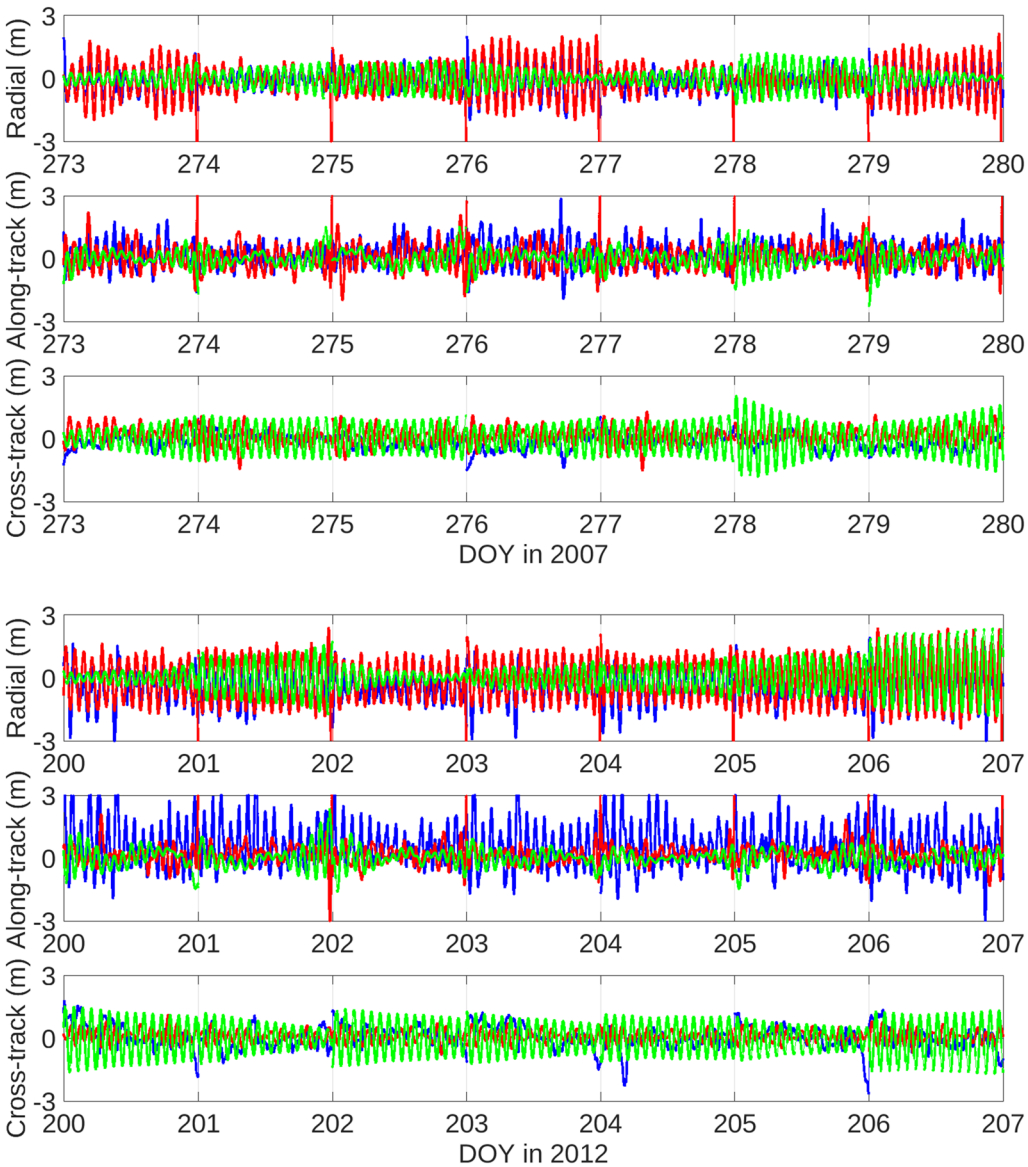

Fig. 5 GRACE-A orbit difference derived by the CL in green, C1 in red and the L1 in blue during the LSA (top) and the HSA (bottom)

Table 3 STD of the orbit difference (in m) for GRACE-A during the low solar activities (DOY 273–279, 2007) and the high solar activities (DOY 200–206, 2012)

	LSA			HSA		
	Radial	Along-track	Cross-track	Radial	Along-track	Cross-track
C1	0.96	0.74	0.43	1.14	0.57	0.29
L1	0.57	0.60	0.38	0.88	1.22	0.53
CL	0.38	0.39	0.56	0.47	0.38	0.60

large in the HSA case, even for the CL observation, as compared to that in the LSA case. The ratio of the CL is fully identical to that of the L1 due to the fact that the CL observation is originated from the L1 (see Eq. (9)). As a result, the occurrence of the cycle slips in LSA is different

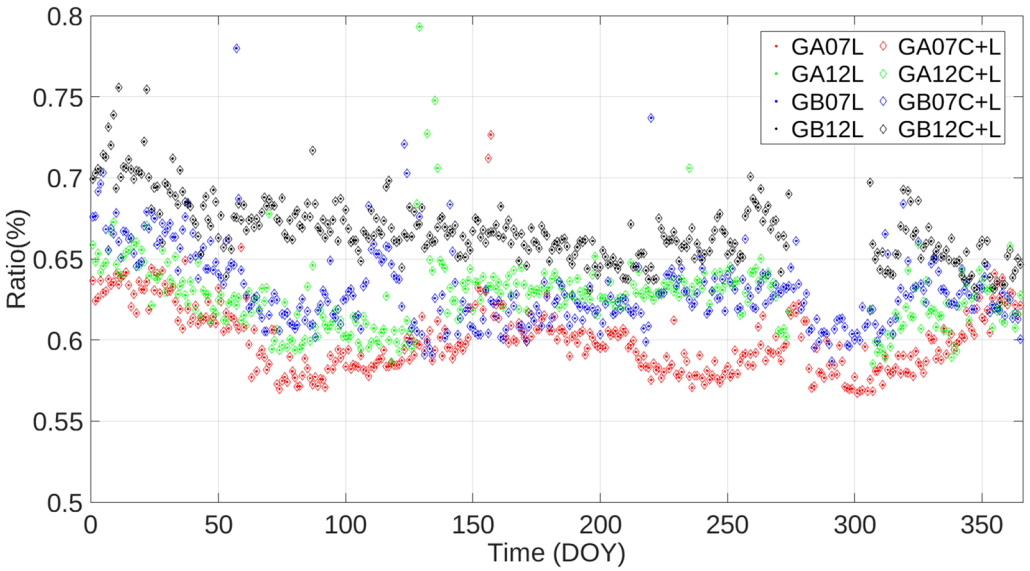

Fig. 6 Ratio between the number of the ambiguity and the number of the observations in both the LSA (2007) case and the HSA (2012) case. Here, C + L (diamond) and L (dot) stands for the CL and L1, respectively; GA sand GB stands for the GRACE-A and GRACE-B, respectively

from that in HSA, suggesting the L1 phase is mainly dominated by the variation of the electron density.

As a final remark, regarding the satellite attitude issue, the GRACE is equipped with the star tracker for the satellite attitude control and the phase wind-up effect is thus effectively minimized (Kang et al. 2006). As such, the error caused by such a phase wind-up effect can be ignored in the SF POD. Besides, the multipath effect can be mitigated by using a choke-ring POD antenna onboard the GRACE (Hwang et al. 2010). On the other hand, the current GIM resulted from an assumption that the ionosphere is condensed in a thin shell with an altitude of 400–450 km above the mean sea level. Such an assumption is not physically true because the ionosphere can be divided into several layers along the electron density profile (Tseng et al. 2021). This GIM model may not be effectively used for the SF-derived orbit solution of LEO satellite above an altitude of 450 km, e.g., GRACE satellites. As a result, the orbit accuracy derived by the L1 measurement varies with the different solar activities and the L1 phase data are not recommended to be used for the SF POD during the HSA.

5 Time synchronization error during the LSA and HSA

The time synchronization is crucial for the application of the LEO + 5G communication. In this section, we assess the time synchronization error from the POD during the different solar activities. The time synchronization is part of the POD procedure and is mainly implemented using the code measurement, which is capable of directly accessing the GPS time having an offset with the UTC time system. In comparison, the phase ambiguity prevents the time of the phase measurement in connection to the GPS time. Here, we design two solutions to see the impact of the different solar activities on the time synchronization solution: the C1-only (termed C1) and the C1 + L1 (termed L1 in this work). For the former, we use the C1-only to direct estimate the time synchronization. For the latter, the C1 is used to estimate the initial value of the time synchronization and the L1 is used to estimate the correction to the initial value.

Figure 7 shows the time synchronization errors for the GRACE-B on DOY 134–135, 2007 and 2012. In this data analysis, the pattern of the time synchronization can be observed when the different observations are used. The time synchronization error derived by the L1 is more perturbed than that derived by the C1. Additionally, the L1 solution in 2012 is much more biased and drifted than that in 2007. In the C1 case for 2012, the periodic variation of the time synchronization error is associated with the orbit period, which is approximate to 90–100 min, resulting in 15 cyclers per day. In comparison, the C1 error variation in 2007 is insignificant due to the low solar condition. Overall, the C1 solution maintains a more consistent time synchronization from time to time than the L1 does. Furthermore, the Cl solution also shows a relatively small discontinuity at the day boundary (UTC 0 h), as compared to the L1 solution. This may be thanks to the code has a strong signal-to-noise in GNSS signal spectra and is modulated

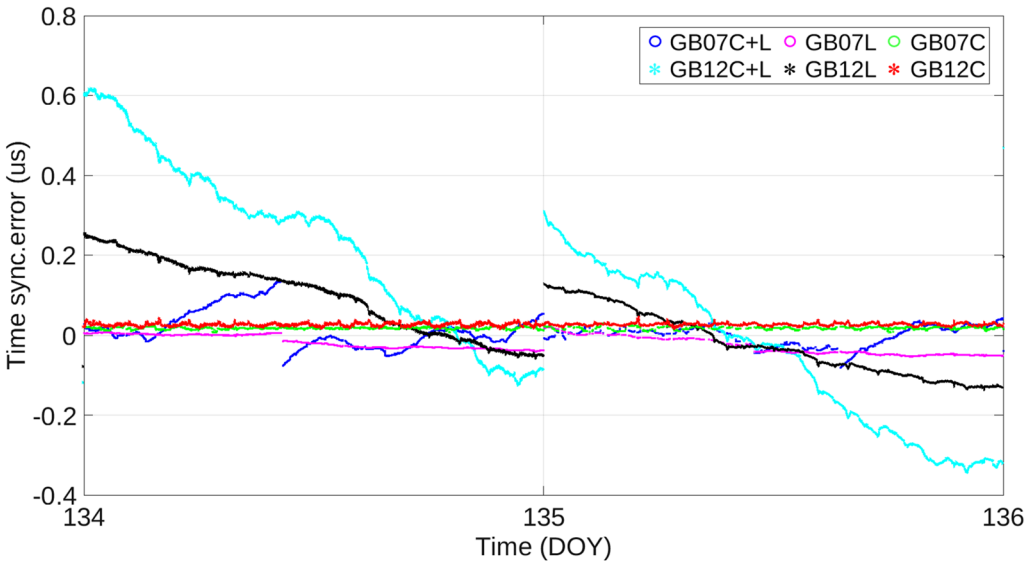

Fig. 7 Time synchronization errors for the GRACE-B on DOY 134–135, 2007 and 2012. GB stands for GRACE-B; L and C stands for L1 and C1, respectively; C + L stands for the CL

on the phase using the Binary Phase Shift Keying (BPSK) technique. The BPSK is a simply modulation technique for GPS radio navigation signals, in which the carrier phase is shifted by 0° and 180°. The BPSK technique only can transmit one bit per symbol, making it easy to implement and less prone to errors. Furthermore, the BPSK provide a high resistance to interference and noise in severe environments, such as high ionosphere activities. In a spread spectrum of the GPS L1 signal, the C1 code has the biggest power than others (Table 7.4 and Fig. 7.8 in Hegarty 2017).

On the other hand, we also design a time synchronization error derived by the CL for comparison. The drifting pattern of the CL-derived time error is similar to that of the L1-derived one. Since the CL has a relatively large noise as compared to the L1 (Eq. (12)), the time discontinuity at the day boundary is more deviated. Note that a clear time discontinuity for the CL (blue) and the L1 (purple) near the middle of DOY 134 in 2007 is commonly found. This is because the data processing for the CL is identical to that for the L1 (also see Fig. 6). Although the GRAPHIC combination is helpful for improving the positioning accuracy, the time error may be deviated if the cycle slip occurs. As a result, a phase-like observation is not recommended for the 5G communication or the SatCom application, which requires the continuity in time synchronization.

Figure 8 shows the Allan deviation for the time synchronization error of GRACE-B using L1, CL and C1 on DOY 134, 2007 and 2012. The Allan deviation is generally used to account for the clock stability, which resulted from the clock estimation (Tseng et al. 2018). The short-term stability of the L1 solution is better than that of the Cl solution. This is because the Allan deviation is mainly based on a relatively stable variation. Besides, the noise of the L1 is smaller than that of the C1, resulting in the relatively good stability. However, this does not indicate that the L1 solution is suggested for the time synchronization application. This is due to the fact that phase ambiguity prevents the receiver clock from accessing to the absolute time system. On the other hand, the stability in the CL case is similar to that in the C1 case for 2007 and 2012. This is mainly caused by the CL noise, which is half of the code noise (see Eq. (12)). Additionally, the long-term stability of the C1 solution is better than that of the L1 solution. This is attributed to the data continuity, indicating that the code observation is free from the cycle slip.

Figure 9 shows the time synchronization error for 2007 and 2012 and Table 4 shows the statistic information with the outliers of 1.0 μs removed. For the time synchronization of the 5G communication, the end-to-end absolute time error is expected within ± 130 ns in support to a 260 ns time error of the signal propagation (Li et al. 2017; Mahmood et al. 2019). That is, the time synchronization error between two reference/base stations, e.g., GPS satellite and LEO satellite, shall be adjusted in a range of ± 130 ns. With such a requirement of the time error, the L1-derived time synchronization in the HSA case may exceeds, potentially leading to a degraded communication

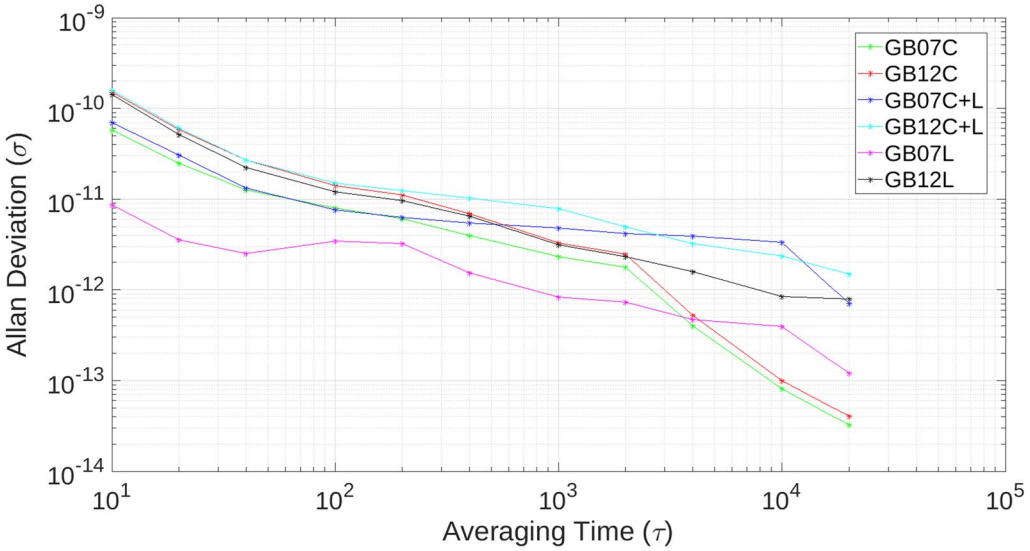

Fig. 8 Allan deviation for the time synchronization error of GRACE-B using L1, CL and C1 on DOY 134, 2007 and 2012. GB stands for GRACE-B; L and C stands for L1 and C1, respectively; C + L stands for the CL

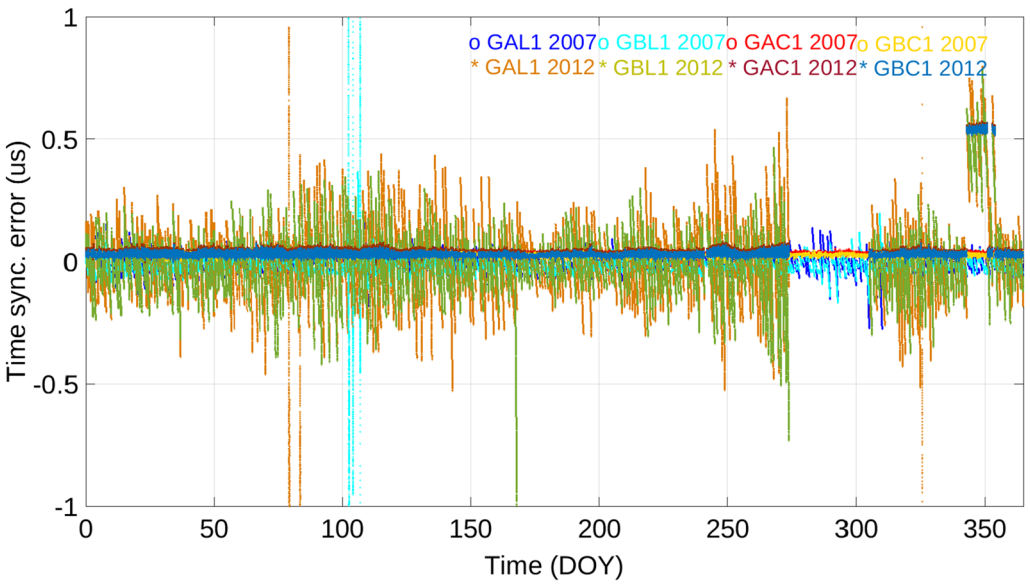

Fig. 9 Time synchronization error of the GRACE satellites for 2007 and 2012. GAC1 and GAL1 stands for the results of GRACE-A using C1 and L1, respectively; GBC1 and GBL1 stands for the results of GRACE-B using C1 and L1, respectively

Table 4 Statistic information of the time synchronization for the GRACE satellites in 2007 and 2012

Satellite	GRACE-A				GRACE-B			
Year	2007		2012		2007		2012	
Types of obs	C1	L1	C1	L1	C1	L1	C1	L1
Mean (ns)	35	− 6	34	− 1	26	− 13	26	− 1
STD (ns)	4	33	6	126	4	28	6	112
RMS (ns)	35	34	35	126	26	31	27	112

application. On the other hand, for 5G positioning service, the relative time error with respect to the reference/base station is required to be ± 10 ns. In this sense, the relative time synchronization error for a combination of the LEO + 5G terrestrial network shall also be adjusted within the range of ± 10 ns. In Table 4, the C1-derived STD much more meets such a requirement of the relative time error that the L1-derived STD. Furthermore, in Fig. 9, the C1 generates a relatively consistent time synchronization error as compared to the L1 for 2007 and 2012. This strongly suggests that the C1 is more suitable for the time synchronization applications than the L1.

6 Conclusions

The major objective of this work is to provide the consistent solution of the satellite orbit and time synchronization during the different solar activities. The different solar activities lead to the ionosphere perturbation, leading to the different occurrence probability of ionospheric irregularities. The ionospheric irregularity affects the amplitude and phase of GPS signal, which can be indexed by the S4 value. We determine the GRACE satellite orbit using the SF GPS observations and compare the resulting orbit to that derived by dual-frequency observations for the effectiveness. The L1 sigma is relatively small in 2007 as compared to the C1 one, whereas the L1 sigma in 2012 is larger and more divergent than the C1 one. On the other hand, the orbit difference derived by L1 during the HSA is much worse than that during the LSA by ~ 1 m. In comparison, the orbit difference derived by C1 during the HSA is consistent with that during the LSA. On the other hand, we also present the data analysis of a ratio between the number of ambiguities and the number of phase observations. The occurrence of the cycle slips in the LSA case is different from that in the HSA case, indicating that the L1 phase is mainly dominated by the variation of the electron density.

On the other hand, the ionospheric correction can be derived from the combination of code and phase observations, e.g., (L1-C1)/2. However, this does not work well for GPS because the code is typically too noisy. In contrast, for Galileo (e.g., Sentinel-6), this can be an option to derive an ionospheric correction. Installing a Galileo receiver onboard LEO may lead even to better POD results than when using GPS (Montenbruck et al. 2021). Such a research topic may be left for a future work.

Regarding the data analysis of the time synchronization, the C1 solution maintains a more consistent time synchronization over time than the L1 solution does. Furthermore, the Cl solution also shows a relatively small discontinuity at the day boundary, as compared to the L1 solution. On the other hand, we also present the time synchronization error using the GRAPHIC combination. Such a combination is intrinsically phase-like, which prevents the receive clock from the absolute time due to the phase ambiguity. This strongly suggests that the C1 is more suitable for the time synchronization applications than the L1 during the LSA and HSA. Last but not least, the GRACE is dedicated for satellite geodetic research and equipped with high-quality scientific instruments, such as star tracker and ultra-stable oscillator, for the POD-related tasks. This implies that the results shown in this work is optimal. For the commercial commutation purpose, the LEO communication satellite may not equip with such high-quality instruments for the POD, perhaps leading to the relatively degraded solution. This study serves as a reference for the applications using the SF POD.

Acknowledgements

This study is funded by the National Science and Technology Council under project number NSTC 112-2121-M-006 -011, NSTC 111-2121-M-992 -001 and NSTC 111-2628-E-006 -009 -MY3. We are grateful for the CODE Analysis Center for providing the GPS orbits and earth orientation parameters. We thank two anonymous reviewers for improving the paper quality.

Author contributions

TT initialized the main idea and wrote the main manuscript text. TT, WY, YT and TH worked on data analysis. YT and PK worked on the data collection. KL and YH commented on the manuscript.

Availability of data and materials

The GRACE data are available at ftp://isdcftp.gfz-potsdam.de/grace. The F10.7 Data download link is referred to https://spdf.gsfc.nasa.gov/pub/data/omni/low_res_omni/. On the other hand, the GPS satellite orbit is downloaded from http://ftp.aiub.unibe.ch/CODE/.

Declarations

Competing interests

The authors declare no competing interests.

Author details

[1]Department of Geomatics, National Cheng Kung University, 1, University Road, Tainan 701, Taiwan. [2]Taiwan Space Agency, Hsinchu, Taiwan. [3]Accelerator Lab., Nuclear Science and Technology Development Center, National Tsing Hua University, Hsinchu, Taiwan. [4]Department of Soil and Water Conservation, National Chung Hsing University, Taichung, Taiwan.

Received: 30 January 2024 Accepted: 12 June 2024
Published online: 28 June 2024

References

Beutler G, Jäggi A, Hugentobler U, Mervart L (2006) Efficient satellite orbit modelling using pseudo-stochastic parameters. J Geod 80:353–372. https://doi.org/10.1007/s00190-006-0072-6

Bock H, Jäggi A, Dach R, Beutler G (2009a) GPS single-frequency orbit determination for low earth orbiting satellites. Adv Space Res 43:783–791. https://doi.org/10.1016/j.asr.2008.12.003

Bock H, Dach R, Jäggi A, Beutler G (2009b) High-rate GPS clock corrections from CODE: support of 1 Hz applications. J Geod 83:1083–1094. https://doi.org/10.1007/s00190-009-0326-1

Briggs BH, Parkin IA (1963) On the variation of radio star and satellite scintillations with zenith angle. J Atmos Terr Phys 25(6):339–366. https://doi.org/10.1016/0021-9169(63)90150-8

Chen SP, Liu JY, Lin CCH, Yeh WH (2021) A global model for the occurrence probability of L-band scintillation S4-index. Terr Atmos Ocean Sci 32(6):977–987. https://doi.org/10.3319/TAO.2021.08.10.03
Dach R, Brockmann E, Schaer S, Beutler G, Meindl M, Prange L, Bock H, Jäggi A, Ostini L (2009) GNSS processing at CODE: status report. J Geod 83:353–366. https://doi.org/10.1007/s00190-008-0281-2
Dach R, Lutz S, Walser P, Fridez P (eds) (2015) Bernese GNSS software version 5.2. User manual, Astronomical Institute, University of Bern, Bern Open Publishing, Bern
Giambene G, Kota S, Pillai P (2018) Satellite-5G integration: a network perspective. IEEE Netw 32(5):25–31. https://doi.org/10.1109/MNET.2018.1800037
Guidotti A et al (2017) Satellite-enabled LTE systems in LEO constellations. 2017 IEEE International Conference on Communications Workshops (ICC Workshops), Paris France, pp 876–881
Hegarty CJ (2017) The global positioning system (GPS). In: Teunissen PJG, Montenbruck O (eds) Springer handbook of global navigation satellite systems. Springer, Cham, pp 933–964
Hwang C, Tseng TP, Lin T, Švehla D, Schreiner B (2009) Precise orbit determination for the FORMOSAT-3/COSMIC satellite mission using GPS. J Geod 83:477–489. https://doi.org/10.1007/s00190-008-0256-3
Hwang C, Tseng TP, Lin TJ, Švehla D, Hugentobler U, Chao BF (2010) Quality assessment of FORMOSAT-3/COSMIC and GRACE GPS observables: analysis of multipath, ionospheric delay and phase residual in orbit determination. GPS Solut 14:121–131. https://doi.org/10.1007/s10291-009-0145-0
Kang Z, Tapley B, Bettadpur S, Ries J, Nagel P, Pastor R (2006) Precise orbit determination for the GRACE mission using only GPS data. J Geod 80:322–331. https://doi.org/10.1007/s00190-006-0073-5
Kang Z, Tapley B, Chen J, Ries J, Bettadpur S (2009) Geocenter variations derived from GPS tracking of the GRACE satellites. J Geod 83:895–901. https://doi.org/10.1007/s00190-009-0307-4
Kato N et al (2019) Optimizing space-air-ground integrated networks by artificial intelligence. IEEE Wirel Commun 26(4):140–147. https://doi.org/10.1109/MWC.2018.1800365
Kodheli O, Guidotti A, Vanelli-Coralli A (2017) Integration of satellites in 5 G through LEO constellations. GLOBECOM 2017 - 2017 IEEE Global Communications Conference, Singapore, pp 1–6. https://doi.org/10.1109/GLOCOM.2017.8255103
Kursinski ER, Hajj GA, Schofield JT, Linfield RP, Hardy KR (1997) Observing earth's atmosphere with radio occultation measurements using the global positioning system. J Geophys Res: Atmospheres 102(D19):23429–23465. https://doi.org/10.1029/97JD01569
Li H, Han L, Daun R, Garner GM (2017) Analysis of the synchronization requirements of 5G and corresponding solutions. IEEE Communi Std Mag 1(1):52–58. https://doi.org/10.1109/MCOMSTD.2017.1600768ST
Liu JY, Chen SP, Yeh WH, Tsai HF, Rajesh PK (2016) Worst-case GPS scintillations on the ground estimated from radio occultation observations of FORMOSAT-3/COSMIC during 2007–2014. Surv Geophys 37:791–809. https://doi.org/10.1007/s10712-015-9355-x
Lyard F, Lefevre F, Letellier T, Francis O (2006) Modelling the global ocean tides: modern insights from FES2004. Ocean Dyn 56:394–415. https://doi.org/10.1007/s10236-006-0086-x
Mahmood A, Ashraf MI, Gidlund M, Torsner J, Sachs J (2019) Time synchronization in 5G wireless edge: requirements and solutions for critical-MTC. IEEE Commun Mag 57(12):45–51. https://doi.org/10.1109/MCOM.001.1900379
Montenbruck O, Ramos-Bosch P (2008) Precision real-time navigation of LEO satellites using global positioning system measurements. GPS Solut 12:187–198. https://doi.org/10.1007/s10291-007-0080-x
Montenbruck O, Hackel S, Wermuth M et al (2021) Sentinel-6A precise orbit determination using a combined GPS/Galileo receiver. J Geod 95:109. https://doi.org/10.1007/s00190-021-01563-z
Pavlis NK, Holmes SA, Kenyon SC, Factor JK (2012) The development and evaluation of the earth gravitational model 2008 (EGM2008). J Geophys Res 117:B04406. https://doi.org/10.1029/2011JB008916
Petit G, Luzum B (2010) IERS Conventions (2010). IERS Technical Note No.36 Verlag des Bundesamt für Kartographie und Geodesie Frankfurt am Main 2010.
Phinney RA, Anderson DL (1968) On the radio occultation method for studying planetary atmospheres. J Geophys Res: Space Phys 73(5):1819–1827. https://doi.org/10.1029/JA073i005p01819
Rebischung P, Griffiths J, Ray J, Schmid R, Collilieux X, Garayt B (2012) IGS08: the IGS realization of ITRF2008. GPS Solut 16:483–494. https://doi.org/10.1007/s10291-011-0248-2
Ruan Y, Li Y, Wang CX, Zhang R (2018) Energy efficient adaptive transmissions in integrated satellite-terrestrial networks with SER constraints. IEEE Trans Wireless Commun 17:210–222. https://doi.org/10.1109/TWC.2017.2764472
Schreiner WS, Sokolovskiy SV, Rocken C, Hunt DC (1999) Analysis and validation of GPS/MET radio occultation data in the ionosphere. Radio Sci 34(4):1005–1003. https://doi.org/10.1029/1999RS900034
Strugarek D, Sośnica K, Jäggi A (2019) Characteristics of GOCE orbits based on satellite laser ranging. Adv Space Res 63(1):417–431. https://doi.org/10.1016/j.asr.2018.08.033
Tseng TP, Hwang C, Yang SK (2012) Assessing attitude error of FORMOSAT-3/COSMIC satellites and its impact on orbit determination. Adv Space Res 49(9):1301–1312. https://doi.org/10.1016/j.asr.2012.02.007
Tseng TP et al (2014) Assessing antenna field of view and receiver clocks of COSMIC and GRACE satellites: lessons for COSMIC-2. GPS Solut 18:219–230. https://doi.org/10.1007/s10291-013-0323-y
Tseng TP, Hwang C, Sośnica K, Kuo CY, Liu YC, Yeh WH (2017) Geocenter motion estimated from GRACE orbits: the impact of F10.7 solar flux. Adv Space Res 59(11):2819–2830. https://doi.org/10.1016/j.asr.2016.02.003
Tseng TP, Chen SY, Chen KL, Huang CY, Yeh WH (2018) Determination of near real-time GNSS satellite clocks for the FORMOSAT-7/COSMIC-2 satellite mission. GPS Solut. https://doi.org/10.1007/s10291-018-0714-1
Tseng TP, Shum CK, Hsiao YS, Kuo CY, Yeh WH (2021) Impact of semi-annual ionospheric total electron content variation on station displacements using single-frequency PPP. Terr Atmos Ocean Sci 32(4):541–551. https://doi.org/10.3319/TAO.2021.08.31.01
Wang W, Chen T, Ding R, Seco-Granados G, You L, Gao X (2021) Location-based timing advance estimation for 5g integrated leo satellite communications. IEEE Trans Veh Technol 70(6):6002–6017. https://doi.org/10.1109/TVT.2021.3079936
Yeh WH et al (2022) Introduction of TROPS ionospheric TEC products for FORMOSAT-7/COSMIC-2 mission. Terr Atmos Ocean Sci. https://doi.org/10.1007/s44195-022-00027-x
Yunck TP (1996) Orbit determination. In: Parkinson BW, Enge P, Axelrad P, Spilker JJ (eds) Global positioning system: theory and applications, vol II. American Institute of Aeronautics and Astronautics (AIAA) Publications, Washington D C

Publisher's Note